

Reactivity in Nucleophilic Vinylic Substitution (S_NV): $S_NV\pi$ versus $S_NV\sigma$ Mechanistic Dichotomy

Israel Fernández,[†] F. Matthias Bickelhaupt,[‡] and Einar Uggerud^{§,*}

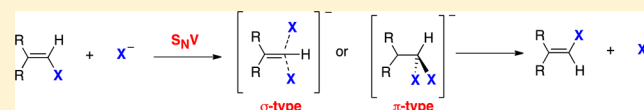
[†]Departamento de Química Orgánica, Facultad de Química, Universidad Complutense, 28040-Madrid, Spain

[‡]Department of Theoretical Chemistry, Amsterdam Center for Multiscale Modeling, VU University Amsterdam, De Boelelaan 1083, NL-1081 HV Amsterdam, The Netherlands, and Institute of Molecules and Materials, Radboud University Nijmegen, Heyendaalseweg 135, NL-6525 AJ Nijmegen, The Netherlands

[§]Massespektrometrlaboratoriet og Senter for teoretisk og beregningsbasert kjemi (CTCC), Kjemisk institutt, Universitetet i Oslo, Postboks 1033 Blindern, N-0315 Oslo, Norway

Supporting Information

ABSTRACT: The intrinsic electronic factors that determine reactivity in prototypical identity nucleophilic vinylic substitution reactions, $X^- + ViX \rightarrow XVi + X^-$ ($Vi = \text{vinyl}$), have been studied by performing quantum chemical calculations (OPBE/6-311++G(d,p)). Of the two limiting reaction types

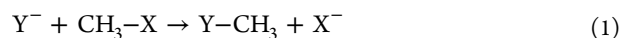


envisaged—the $S_NV\pi$ and $S_NV\sigma$ mechanisms—the former is preferred for most combinations of nucleophiles and substrates, except for the combination of unactivated substrates and poor nucleophiles, as seen for the much studied reactions $Cl^- + CH_2CHCl$ and $Br^- + CH_2CHBr$. It was found that periodic trends for $S_NV\pi$ are essentially the same as those previously reported for nucleophilic aromatic substitution, S_NAr , while intrinsic $S_NV\sigma$ nucleophilicity parallels aliphatic S_N2 . It is therefore concluded that S_NV reactivity in general can be understood in terms of this mechanistic dichotomy. Furthermore, a few representative reactions were analyzed applying two complementary schemes for energy decomposition analysis.

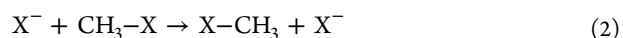
INTRODUCTION

Nucleophilic vinylic substitution (S_NV)¹ is a reaction mechanistic scheme of relevance to many subdisciplines of chemistry including organic synthesis, industrial polymerization and biochemistry.^{2–13} In an S_NV reaction, the nucleophile attacks an sp^2 hybridized carbon atom, the α carbon, whereupon the nucleofuge (leaving group)—originally bonded to the same carbon—eventually leaves. Rappoport has described the mechanistic landscape in detail, noting rich variation involving up to 30 mechanistic subtypes.¹⁴ Computational quantum chemistry studies^{15–29} have clarified this view by showing how the actual mechanistic route followed by a particular reaction depends on the properties of both the nucleophile and substrate. Two limiting mechanisms can be identified, the reaction may either occur by a sideways in-plane attack by the nucleophile ($S_NV\sigma$ or attack from above ($S_NV\pi$), Scheme 1. The reaction is generally sluggish unless the substrate molecule is activated by electron-withdrawing substituents (R) at the β carbon, and the reaction can either occur in a single step or in a step-by-step fashion. In the limiting $S_NV\sigma$ mechanism, which on the basis of an early computational study²³ seems to be energetically preferred for nonactivated substrates, the reaction occurs in one step with concerted formation of the bond to the nucleophile and fracture of the bond to the nucleofuge, while limiting $S_NV\pi$ more typical for activated substrates,²⁶ involves the intermediate formation of a covalently bonded carbanion adduct of the two reacting species.

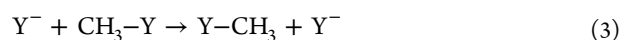
In previous papers, gas phase aliphatic S_N2 reactivity has been systematically addressed by applying various quantum chemical methods and approaches.^{30–43} These studies have demonstrated how trends in reactivity can be examined in terms of physical observables and other well-defined parameters, relating these to periodic table order. The prototype reaction,



has been studied in great detail, and it has been shown^{44–48} that the critical energy (E^\ddagger , the energy difference between the transition state and the isolated reactants) necessary to adapt the transition state geometry has two contributions, one from the thermochemical driving force (the bond dissociation energy difference between the $C-Y$ bond to be formed and the $C-X$ bond to be broken) and another from an intrinsic factor that is equal to the average critical energy of the two identity reactions, i.e., the corresponding reactions in which the nucleophile and nucleofuge are identical:



and

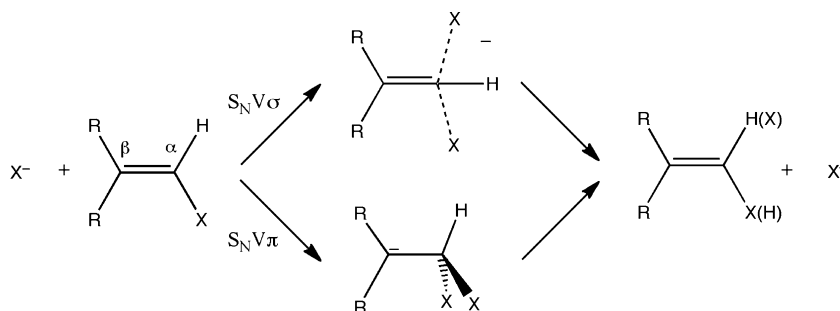


The two factors can readily be separated applying quantitative Bema Hapothle formalism.⁴⁹ Along one period of

Received: June 13, 2013

Published: August 5, 2013

Scheme 1



the periodic table, intrinsic reactivity increases from left to right, meaning that the barrier heights for the identity reactions follow the trend $\text{NH}_2^- > \text{OH}^- > \text{F}^-$, decreasing linearly with decreasing proton affinity of the nucleophile/nucleofuge.³¹ However, there is relatively little variation within one group, for example, $\text{F}^- \approx \text{Cl}^- \approx \text{Br}^-$, although the barrier still decreases along this series.

The above trends can also readily be understood in terms of the ball-in-a-box (BIB) model. This model is based on the finding that the five groups surrounding the pentacoordinate carbon in the labile transition state are in contact. They cannot approach each other more closely without causing repulsion as a consequence of their overlapping wave functions. Typically, this constitutes a “box of substituents” with a cavity in which the relatively small carbon atom cannot form a favorable (i.e., short enough) bond to X and Y simultaneously: it can either bind tightly X or to Y. Crossing from X via the center of the cavity to Y is therefore energetically unfavorable. The energetic punishment associated with carbon crossing the center of the box of substituent and thus the $\text{S}_{\text{N}}2$ barrier drops, as the affinities^{50,51} of X or Y for carbon decrease. This is exactly what happens along $\text{NH}_2^- > \text{OH}^- > \text{F}^-$ and to a lesser extent also along $\text{F}^- > \text{Cl}^- > \text{Br}^-$.

More recently, the Bema Hapothle formalism was applied for analyzing reactivity in nucleophilic aromatic substitution reactions, the $\text{S}_{\text{N}}\text{Ar}$ reaction.⁵² It was found that the critical energy of the identity reaction $\text{X}^- + \text{PhX} \rightarrow \text{XPh} + \text{X}^-$ (Ph = phenyl) shows the following trend: $\text{NH}_2^- \approx \text{OH}^- \approx \text{F}^- \ll \text{PH}_2^- \approx \text{SH}^- \approx \text{Cl}^- \ll \text{AsH}_2^- \approx \text{SeH}^- \approx \text{Br}^-$. For period 2 nucleophiles/nucleofuges, the Ph(X)_2^- species corresponds to a potential energy minimum (Meisenheimer complex) and consequently E^\ddagger is negative, while for period 4, it is a saddle point (a TS). These trends are clearly different from those found for the aliphatic $\text{S}_{\text{N}}2$ reaction, so aromatic and aliphatic intrinsic reactivities are therefore of dissimilar kinds.

On the basis of these considerations, it became pertinent also to analyze the $\text{S}_{\text{N}}\text{V}$ reaction in terms of intrinsic reactivity, and see how it is related to aliphatic and aromatic substitution, respectively—in particular, how closely $\text{S}_{\text{N}}\text{V}\sigma$ and $\text{S}_{\text{N}}\text{V}\pi$ relate to $\text{S}_{\text{N}}2$ and $\text{S}_{\text{N}}\text{Ar}$, respectively. Moreover, it is also of interest to investigate more closely the intrinsic reactivity factors that determine the mechanistic preference, and to determine the point of crossover from $\text{S}_{\text{N}}\text{V}\sigma$ to $\text{S}_{\text{N}}\text{V}\pi$. Our study has two parts. In the first part, we investigate the role of the nucleophile/nucleofuge and the substrate in order to identify periodic reactivity trends. In the second part, we apply bond energy decomposition analysis to typical limiting $\text{S}_{\text{N}}\text{V}$ reactions to discover the continuous change in the essential components along the entire reaction path to see how the electronic contributions play together.^{53–55}

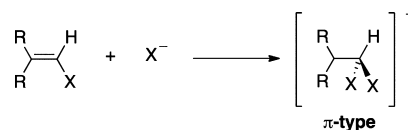
METHODS

Molecular geometries were optimized using DFT theory applying the OPBE functional.^{56,57} This choice of method is partly dictated by the fact that it has been demonstrated to provide good accuracy in reproducing important physical parameters including reaction barriers,^{38,58} and partly because we used it for our previous analysis of $\text{S}_{\text{N}}2$ and $\text{S}_{\text{N}}\text{Ar}$ reaction energetics.^{33,52} The basis set used, 6-311++G(d,p), has triple- ζ quality augmented by two sets of polarization functions and two diffuse functions. This level of theory is denoted OPBE/6-311++G(d,p). Vibrational frequencies of all optimized structures were calculated to inspect the nature of the stationary points (minimum or transition structure). The calculations were carried out with the GAUSSIAN 03 suite of programs.⁵⁹

The potential energy surface (PES) along the model reaction coordinate was analyzed in two ways: (i) in terms of the nucleophile/nucleofuge pair interacting with the carbocationic remainder of the reaction system, designated Reference I; (ii) in terms of the reactants, i.e., the nucleophile interacting with the substrate molecule (designated Reference II). Note that Reference II is identical to the activation strain model for bimolecular reactions.^{60,61} The interactions between the fragments (i.e., $[\text{X}^-\text{X}]^{2-} + \text{R}_2\text{C}=\text{CH}^+$ in Reference I; $\text{X}^- + \text{R}_2\text{C}=\text{CHX}$ in Reference II) were analyzed by means of the scheme for energy decomposition analysis (EDA) contained in the ADF program package.⁶² This scheme was developed by Ziegler and Rauk.⁶³ It is similar to, but also differs in some points from, the procedure proposed by Morokuma.^{64–66} Briefly explained, the scheme is set up for analyzing the interaction between two fragments in terms of the instantaneous interaction energy, ΔE_{int} defined to be the energy difference between the supermolecule describing the system of interest and the separated fragments in the same geometric arrangement of atoms they have in the supermolecule and in the proper electronic reference state. The interaction energy can be divided into three main components:

$$\Delta E_{\text{int}} = \Delta E_{\text{elstat}} + \Delta E_{\text{Pauli}} + \Delta E_{\text{orb}} \quad (4)$$

ΔE_{elstat} gives the electrostatic interaction energy between the fragments, which are calculated using the frozen electron density distribution of the fragments in the geometry of the supermolecule. The second term of eq 4, ΔE_{Pauli} , refers to the repulsive interactions between the fragments, which are caused by the fact that two electrons with the same spin cannot occupy the same region in space. ΔE_{Pauli} is calculated by enforcing the Kohn–Sham determinant on the superimposed fragments to obey the Pauli principle by antisymmetrization and renormalization. The stabilizing orbital interaction term, ΔE_{orb} , is calculated in the final step of the energy partitioning analysis when the Kohn–Sham orbitals relax to their optimal form. This term can be further partitioned into contributions by the orbitals belonging to different irreducible representations of the point group of the interacting system. The interaction energy, ΔE_{int} , can be used to calculate the bond dissociation energy, D_e , by adding ΔE_{prep} , which is the energy necessary to promote the fragments from their equilibrium geometry to the geometry in the supermolecule (eq 5). The advantage of using ΔE_{int} instead of D_e is that the instantaneous electronic interaction of the fragments becomes analyzed, which yields a direct

Table 1. Energy and Data Obtained with OPBE/6-311++G(d,p) π -Type Systems

X	R	minimum	TS (ν^\ddagger , cm^{-1}) ^a	E^\ddagger ^b kJ/mol	$E(1s-C)$ ^c Hartrees
F	H		yes (i 324)	-11.3	-9.856
F	CN	yes		-269.9	-9.941
F	NO ₂	yes		-300.4	-9.938
Cl	H		yes (i 451)	+105.0	-9.835
Cl	Cl		yes (i 293)	+63.2	-9.845
Cl	CN	yes		-100.4	-9.907
Cl	NO ₂	yes		-125.9	-9.902
Br	H		yes (i.514)	+106.7	-9.831
Br	Cl		yes (i.274)	+69.4	-9.839
Br	CN	yes		-77.4	-9.899
Br	NO ₂	yes		-201.7	-9.893
OH	H	yes		-43.5	
SH	H		yes (i.409)	+83.2	-9.805
SeH	H		yes (i.369)	+87.0	-9.804
NH ₂	H	yes		-25.5	-9.780
PH ₂	H		yes (i.291)	+29.0	-9.779
AsH ₂	H		yes (i.291)	+40.2	-9.780

^aVibrational frequency corresponding to the reaction coordinate. ^bCritical energy, i.e., energy difference between central complex (Meisenheimer complex or TS) and reactants (zero point energies included). ^cCore electron binding energy of the reaction central carbon atom of the reactant molecule.

estimate of the energy components. Further details about the EDA can be found in the literature.^{67–74}

$$-D_e = \Delta E_{\text{prep}} + \Delta E_{\text{int}} \quad (5)$$

In order to take into account the contribution of dispersion effects, the EDA calculations were performed with the dispersion-corrected DFT-D3 method developed by Grimme and co-workers⁷⁵ in combination with the BLYP^{76,77} functional: BLYP-D3. The molecular orbitals (MOs) were expanded in a large uncontracted set of Slater-type orbitals (STOs) containing diffuse functions, TZ2P. This basis is of triple- ζ quality and has been augmented by two sets of polarization functions, that is, p and d functions for the hydrogen atom and d and f functions for the other atoms. An auxiliary set of s, p, d, f, and g STOs was used to fit the molecular density and to represent the Coulomb and exchange potentials accurately in each SCF cycle. Relativistic effects were accounted for by using the zeroth-order regular approximation (ZORA).⁷⁸

RESULTS AND DISCUSSION

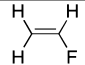
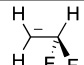
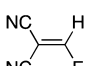
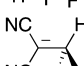
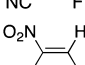
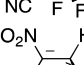
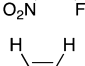
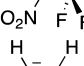
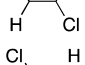
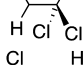
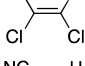
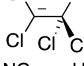
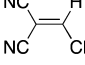
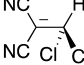
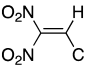
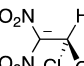
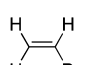
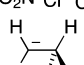
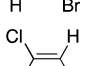
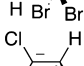
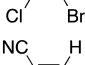
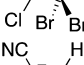
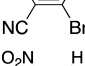
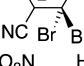
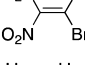
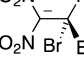
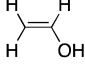
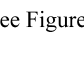
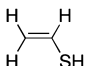
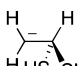
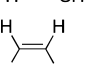
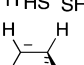
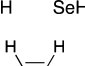
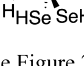
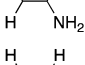
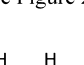
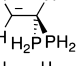
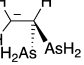

The results of our calculations are summarized in Tables 1–4. For all reaction systems (Figure 1), the perpendicular attack pathway, $S_NV\pi$ (Tables 1 and 2), and the in-plane attack pathway, $S_NV\sigma$ (Tables 3 and 4), were thoroughly investigated to localize all relevant potential energy minima and saddle points. For unactivated substrates CH_2CHX , it is clear that $S_NV\pi$ is the preferred mechanistic route, except for $X = \text{Cl}, \text{Br}$. For all substrates following the $S_NV\pi$ route, except $X = \text{NH}_2$ and OH , the critical symmetrical configuration $\text{CH}_2\text{CH}(\text{X}_2)^-$ corresponds to a saddle point of the potential energy surface (a TS), whereas for $X = \text{NH}_2$ and OH , it is a minimum (see below). Several of the previous quantum chemical studies on nucleophilic vinylic substitution have focused on the mechanisms of halide anion attack on vinyl halide substrates, concluding that the barriers for these reactions are high and that the $S_NV\sigma$ pathway is preferred to the $S_NV\pi$ pathway. As evident from the present results, based on a broader range of

nucleophiles and substrates, we are now able to see that the much studied $X = \text{Cl}$ and Br are rather exceptional and that the π route is the more common.

We also note that for the unactivated substrates ($R = \text{H}$), the critical configuration where the two X groups become equivalent, strongly resembles the Meisenheimer complex of nucleophilic aromatic substitution. For $X = \text{OH}$ and NH_2 , the β carbon changes character and becomes pyramidal, and as a consequence the minimum energy structure of the π adduct has a geometry that is no longer of C_s symmetry. The enforced C_s symmetry to these species leads to transition states which are associated to the pyramidalization of the CH_2 group adjacent to the reactive carbon atom instead to the $\text{C}\cdots\text{X}$ bond breaking/formation (the situation found for the rest of transition states of the $S_NV\pi$ series, see Figure 2). This behavior was noted already by Cohen et al.²² They explained that the rehybridization leads to a more favorable rotation around the C–C bond and that the most stable conformation of the adduct is determined from the optimum hyperconjugative interaction between the emerging carbanionic center at the α carbon and the nucleofuge and nucleophile.

Figure 3 shows the critical energies calculated for the $S_NV\pi$ reactions (Table 1) plotted against the same quantity obtained for S_NAr from Fernández et al.⁵² The plot reveals an approximately linear relationship and also that the critical energies are rather similar for the two reaction types—a finding that substantiates a close mechanistic relationship. Without going into detail here, it can be mentioned that comparison of the bond lengths and angles of substrates and critical configurations of the two reaction types affirms this mechanistic relationship. It is evident from Table 1 that the rehybridization of the α carbon in going from substrate (sp^2) to critical configuration (sp^3) also allows for significantly shorter C–X contacts at the critical configuration of $S_NV\pi$ compared to $S_NV\sigma$. With the exception of chloride and bromide, the

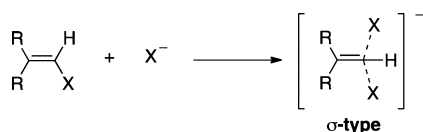
Table 2. Key Geometrical Data Obtained With OPBE/6-311++G(d,p) π -Type Systems

System	r (C=C) / Å	r (C-X) / Å	System	r (C=C) / Å	r (C-X) / Å	X...C...X / degrees
	1.329	1.345		1.396	1.495	95.5
	1.358	1.314		1.464	1.405	102.6
	1.341	1.318		1.478	1.388	105.1
	1.333	1.725		1.359	2.049	96.2
	1.346	1.705		1.365	1.994	98.4
	1.363	1.687		1.444	1.819	104.9
	1.340	1.690		1.457	1.904	108.3
	1.332	1.880		1.351	1.818	108.3
	1.344	1.859		1.358	2.248	96.6
	1.362	1.841		1.423	1.928	104.4
	1.339	1.884		1.443	1.904	108.4
	1.337	1.363			1.986	108.4
	1.340	1.759		1.379	2.015	2.015
	1.339	1.894		1.379	2.186	98.9
	1.346	1.386		1.395	2.186	98.9
	1.340	1.824		1.379	2.196	93.5
	1.338	1.947		1.434	2.187	2.187
				1.457	1.908	113.0
					1.917	
				1.434	2.055	110.8
					2.073	

energetic cost of this rehybridization of the α carbon is therefore outweighed by the stronger C–X interactions allowed for in the Meisenheimer type atomic arrangement.

As already indicated, it is known from the literature that electron-withdrawing substituents at the β carbon activate substrates for vinylic substitution and increase the inclination toward the π route.¹³ The outcome of the present calculations is consistent with this observation. First, we note that for the stronger electron withdrawing substituents, the critical configurations are no saddle points but become minima

(Meisenheimer adducts). Second, we note (Figure 4) how the critical energy decreases when both substituents R = H are exchanged by Cl, CN, and NO₂. The critical energy data are presented as a function of the 1s orbital energy of the α carbon of the substrate in the same manner as in the S_NAr study.⁵² As for para-substituted benzenes in aromatic substitution, we note good linear correlation between E^\ddagger and $E(\text{C}1s)$ for S_NV π for X = H, Cl, and CN, but a deviation from linearity is evident from R = NO₂. This can easily be understood on the basis of simple geometrical arguments; the two nitro-groups cannot achieve

Table 3. Energy and Data Obtained With OPBE/6-311++G(d,p) σ -Type Systems

X	R	TS (ν^\ddagger , cm^{-1}) ^a	E ^{#b} kJ/mol
F	H	i.-593, i.-65	+66.9
F	Cl	i.-569, i.-235	+61.9
F	CN	i.-561, i.-412	-28.0
F	NO ₂	i.-570, i.-209	-16.7
Cl	H	i.-539	+96.6
Cl	Cl	i.-531, i.-99	+135.6
Cl	CN	i.-594, i.-281	+71.5
Cl	NO ₂	i.-556, i.-68	-18.4
Br	H	i.-514	+87.0
Br	Cl	i.-506, i.-52	+127.6
Br	CN	i.-589, i.-260	+70.7
Br	NO ₂	i.-547, i.-36	+77.4
OH	H	i.-651, i.-309, i.-183, i.-118	+151.0
SH	H	i.-605, i.-125	+143.1
SeH	H	i.-591, i.-277, i.-264	+125.9
NH ₂	H	i.-680, i.-235, i.-80	+226.8
PH ₂	H	i.-656, i.-35, i.-23	+174.9
AsH ₂	H	i.-647	+156.9

^aVibrational frequency corresponding to the reaction coordinate.

^bCritical energy, i.e., energy difference between complex and reactants (zero point energies included).

their optimum coplanar positions resulting from the severely congested atomic arrangement of having two nitro-groups bonded to the same carbon. This effect is seen for all systems investigated (F, Cl, and Br).

Having documented the close relationship between of the π pathway of vinylic substitution and aromatic substitution, the next logical step was to examine how the σ pathway resembles aliphatic $\text{S}_{\text{N}}2$ substitution since the critical configurations (transition states) requires related rehybridization of the central α carbon ($\text{sp}^3 \rightarrow \text{sp}^2$ in $\text{S}_{\text{N}}2$ and $\text{sp}^2 \rightarrow \text{sp}$ in $\text{S}_{\text{N}}\text{V}\sigma$). We therefore conducted a series of calculations in which the critical configuration was enforced to C_{2v} symmetry. In this way, we could impose an artificial $\text{S}_{\text{N}}\text{V}\sigma$ reaction also in the systems for which this reaction mechanism is not favorable. By doing so, we could next analyze the critical energy (Table 3) and associated geometries of the sigma transition states (Table 4). In Figure 5, the critical energies are compared to those of the $\text{S}_{\text{N}}2$ reaction.³¹ The barrier of an $\text{S}_{\text{N}}\text{V}\sigma$ reaction is seen to be considerable in all cases, and very interestingly an approximate linear correlation with slope = 2 (not shown in the figure) is inferred. The trends seen in Figures 3 and 5 therefore nicely account for the general preference for $\text{S}_{\text{N}}\text{V}\sigma$.

ACTIVATION STRAIN AND ENERGY DECOMPOSITION ANALYSES

We have applied activation strain analyses (ASA) and energy decomposition analyses (EDA) to allow for examination of the different bonding energy components during the course of a reaction. By conducting geometry optimizations in a step-by-step fashion all the way from reactants to the critical configuration and performing an EDA calculation for optimized geometries, it is possible to find out how the different

Table 4. Key Geometrical Data Obtained with OPBE/6-311++G(d,p) σ -Type Systems

System	r(C=C) / Å	r(C-X) / Å	X...C...X / degrees
	1.325	1.866	162.8
	1.350	1.786	161.6
	1.369	1.729	166.6
	1.329	1.759	169.0
	1.316	2.398	157.6
	1.335	2.380	146.1
	1.356	2.266	157.0
	1.315	2.315	156.7
	1.316	2.554	156.2
	1.330	2.561	142.1
	1.353	2.430	153.1
	1.311	2.494	152.2
	1.328	1.949	166.5
	1.322	2.459	160.7
	1.322	2.582	159.5
	1.330	2.107	159.0
	1.324	2.644	156.5
	1.323	2.735	155.4

contributions to the interaction energy between the selected fragments change as a function of the reaction coordinate. At each point of this well-defined path, the energy components are then computed relative to a predetermined reference system. The choice of the reference system is of course important for the quantitative results but the physical interpretation is equally important. We have chosen to perform our analysis for two different reference systems. The first, Reference I, is defined as the infinitely separated $\text{Vi}^+ + \text{X}^- + \text{X}^-$. This reference was chosen on the basis of previous experience with identity

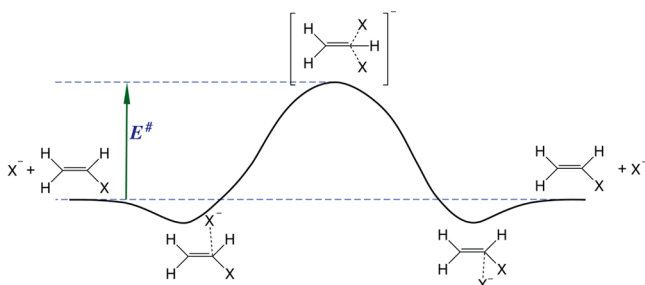


Figure 1. Potential energy curve for a generic vinylic substitution reaction, where ViX is the vinylic substrate and X^- is the nucleophile/nucleofuge. The curve represents an identity reaction where the symmetric geometry corresponds to a saddle point of the potential energy surface. In other cases, the energy of this symmetric species is lower in energy than that of the reactants, or even degenerates into a minimum. In both cases, E^\ddagger will be negative.

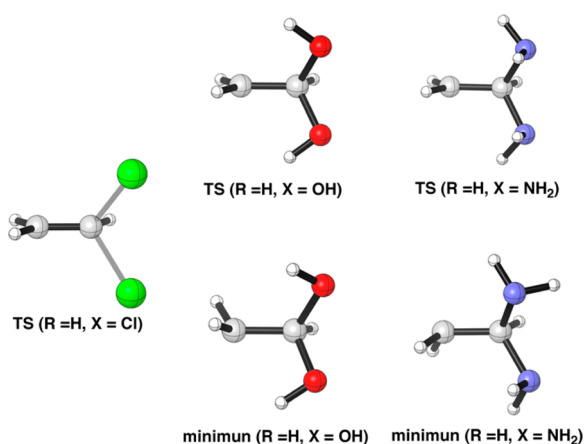


Figure 2. Fully optimized geometries of a typical π -TS ($R = H, X = Cl$), and for the systems involving $R = H, X = OH$, and NH_2 .

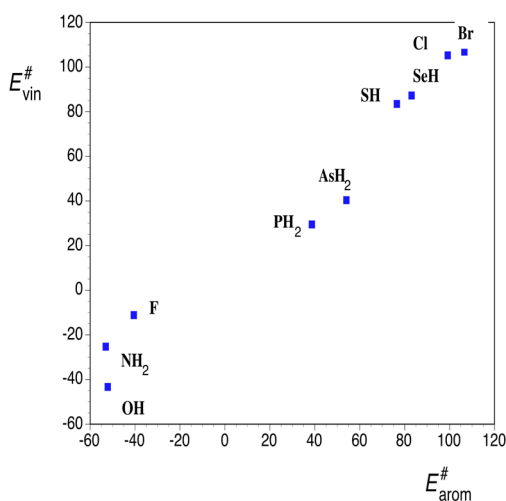


Figure 3. Calculated critical energy (kJ/mol) for vinylic $S_NV\pi$ substitution ($CH_2CHX + X^-$) plotted against the corresponding figure for aromatic $SNAr$ substitution ($PhX + X^-$). The energy data have been taken from Table 1 and ref 9, respectively. The nucleophile/nucleofuge pairs X are indicated.

reactions for which it has turned out useful to consider the critical configuration as a carbocation sandwiched between the equivalent incoming and leaving groups. For practical reasons,

we substitute $X^- + X^-$ by the $[X\cdots X]^{2-}$ dimer. The second reference system, Reference II, is defined as the infinitely separated reactants $ViX + X^-$. Due to the wide mechanistic variation it became necessary to investigate three reactions (a) $H_2CCHCl + Cl^-$ ($S_NV\sigma$) which has a considerable positive critical energy, (b) $H_2CCHCl + Cl^-$ ($S_NV\pi$) with a positive critical energy, and (c) $(NC)_2CCHCl + Cl^-$ ($S_NV\pi$) with a negative critical energy (stable intermediate, Meisenheimer-type complex).

The activation strain analyses (Reference II) reveal a clear pattern that links the preference for unactivated substrate $H_2C=CHCl$ to react via $S_NV\sigma$ to a substantially more favorable ΔE_{int} as the nucleophile approaches the backside of the carbon–leaving group bond than when it approaches the π electron system in the $S_NV\pi$ pathway (compare Figures 6, upper right with middle right). The better interaction compensates for the more destabilizing ΔE_{strain} in the $S_NV\sigma$ pathway that results from the situation that the α -carbon is more crowded, leading to more geometrical deformation, as four substituents have to be accommodated in the same plane. β -cyano substituents activate the substrate by stabilizing the π^* orbitals. This causes a sizable stabilization of the interaction curve ΔE_{int} , among others, through a substantial strengthening of the nucleophile–lone pair \rightarrow substrate π^* orbital interactions contained in ΔE_{orb} (Figure 6, lower right). Consequently, the $S_NV\pi$ pathway becomes viable for such activated substrates.

For reaction (a), both Reference I and II calculations reveal EDA patterns characteristic to those found for S_N2 reactions (Figure 7). For Reference I the positive Pauli repulsion component is relatively constant in the range $r(C\cdots Cl_i) = 4.0 - 2.5 \text{ \AA}$ (distance for incoming nucleophile). The considerable $\Delta E_{Pauli} \approx 920 \text{ kJmol}^{-1}$ at long $C\cdots Cl_i$ distances is mainly due to the exchange repulsion between the vinyl cation moiety and nucleofuge Cl^- in forming H_2CCHCl at the correspondingly short $C\cdots Cl_i$ equilibrium distance within H_2CCHCl . In this range, it seems that any increase in the Pauli repulsion component due to the incoming Cl^- is outweighed by the decrease for the outgoing Cl^- . Close to the transition state geometry, the situation changes quite noticeably and ΔE_{Pauli} drops. It is also noticed that the very favorable electrostatic and orbital attraction terms that are strong at long $r(C\cdots Cl_i)$ decrease close to the critical configuration, clearly showing that these type of attractions are more favorable with one Cl^- tightly bonded to the vinyl cation than two Cl^- at intermediate $C\cdots Cl$ bond lengths, as is the situation in the transition state geometry. For Reference II, the qualitative situation is similar in that the attractive components become weaker the closer one gets to the TS. The most significant quantitative difference lies in the Pauli repulsion term, which increases monotonously in the $r(C\cdots Cl_i) = 4.0 - 2.5 \text{ \AA}$ range. This reflects the significance of the reference system on to the computed component values. We note that the large attractive and repulsive terms (ΔE_{elstat} , ΔE_{Pauli} , ΔE_{orb}) that describe the formation of H_2CCHCl from $H_2CCH^+ + Cl^-$ (Reference I) add up to the rather small ΔE_{prep} term when H_2CCHCl instead is used as reference point (Reference II).

The $S_NV\pi$ and $S_NV\sigma$ mechanisms of reaction (b) have similar critical energies (105 and 97 kJmol^{-1} , respectively, Table 1) and display similar EDA plots. There is, however, one considerable difference in the clearly different approaches to the TS seen for ΔE_{Pauli} . The dip is clearly less pronounced (Reference I) or even absent (Reference II) for $S_NV\pi$ compared to $S_NV\sigma$. However, the results also show that the orbital attraction is

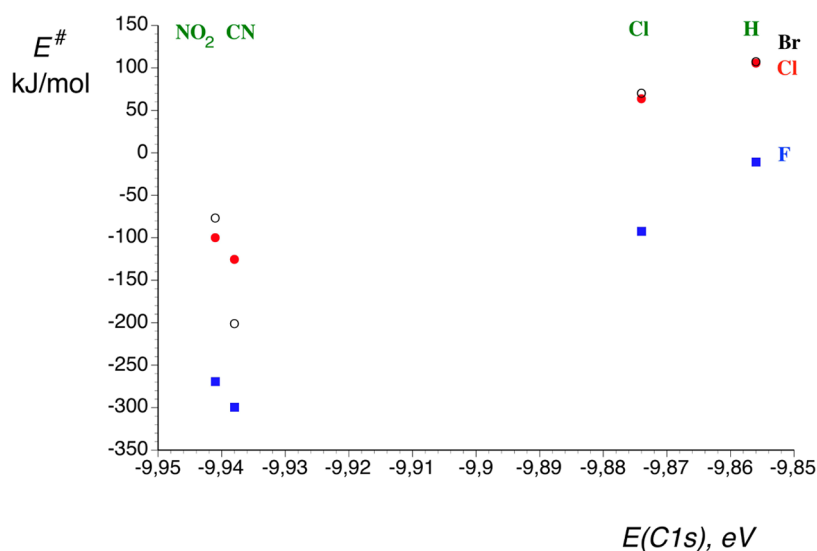


Figure 4. Calculated critical energy (kJ/mol) for vinylic $S_NV\pi$ substitution ($CR_2CHX + X^-$) vs the 1s orbital energy associated with the α carbon of CR_2CHF . The data have been taken from Table 1. Code for data points: Blue filled squares, $X = F$; red filled circles, $X = Cl$; and open black circles, $C = Br$. The R substituents are indicated using green letters.

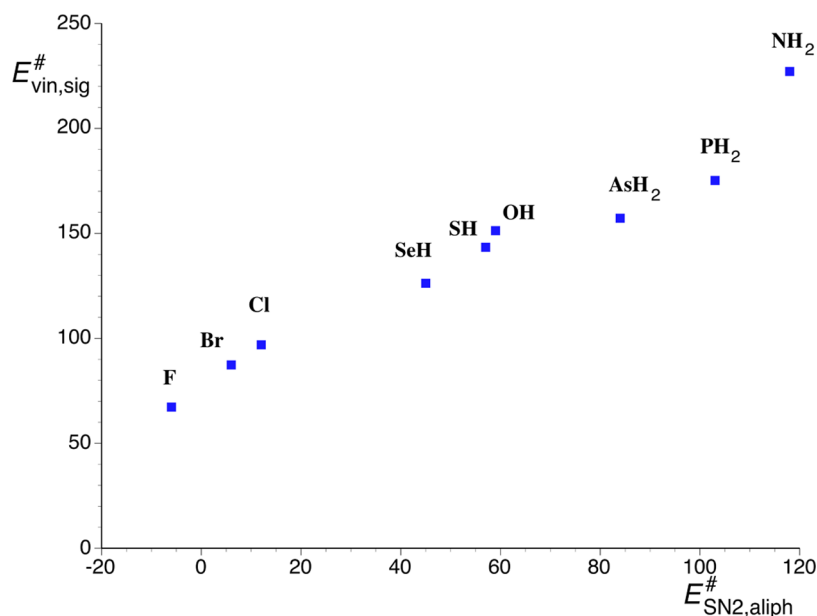


Figure 5. Calculated critical energy (kJ/mol) for vinylic $S_NV\sigma$ substitution ($CH_2CHX + X^-$) plotted against the corresponding figure for aliphatic S_N2 substitution ($CH_3X + X^-$). The energy data have been taken from Table 1 and ref Y, respectively. The nucleophile/nucleofuge pairs X are indicated.

considerably more pronounced for $S_NV\pi$ when compared to $S_NV\sigma$. This is in good accord with the observation that the two C–Cl bonds of the TS are considerably shorter in the former case.

The EDA plot of reaction (c) obtained with Reference I is characteristic for a reaction that has a symmetrical minimum rather than a TS—in complete analogy to what was found for S_NAr .⁴⁴ The Pauli repulsion term increases continuously toward the symmetrical minimum, with a parallel increase in the attractive interactions ΔE_{elstat} and ΔE_{orb} . By direct comparison of the TS parameters of reactions (b) and (c), we observe good consistence between the shorter C–Cl bond length and larger absolute values for ΔE_{elstat} , ΔE_{Pauli} , ΔE_{orb} for the electronically more activated substrate. The Reference II calculations are also typical in displaying similar increase in the absolute values of

the repulsive and attractive terms all the way from reactants to the critical configuration. Finally, the almost negligible contribution of dispersion effects (given by ΔE_{disp}) to the total attraction in S_NV reactions remains practically constant along the reaction coordinate in all of the considered systems (and in both fragmentation schemes)

Although the EDA framework provides a mathematically consistent tool, we will here be humble by not going too far into translating well-defined energy components into more inaccurate chemical terms like electronic effects and steric hindrance. This problem has recently been discussed in a highly readable essay,⁷⁹ and it was wisely pointed out that the pitfalls on this road are many and deep.

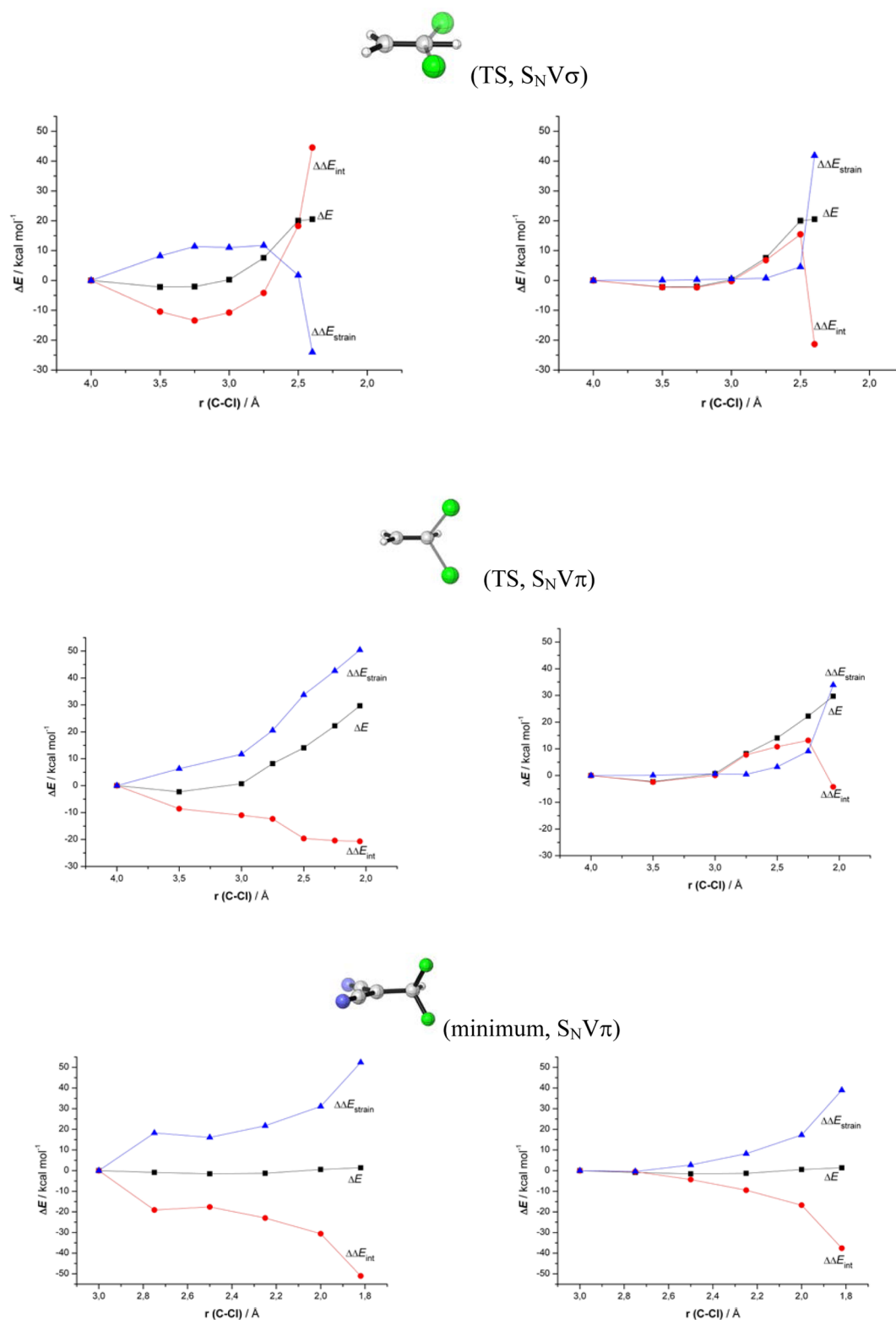


Figure 6. Analyses of reaction profiles ΔE for selected S_NV processes in terms of strain ΔE_{strain} plus interactions ΔE_{int} . Left plots: The fragmentation $[R_2C=CH^+] + [Cl\cdots Cl]^2$; denoted as Reference I in the text. Right plots: the fragmentation $[R_2C=CHCl] + Cl^-$, denoted as Reference II or activation strain model in the text.

CONCLUSIONS

In identity substitution reactions where the attacking and leaving groups are the same, there is no overall thermochemical driving force that otherwise would have made the bonds of the products stronger than in the reactants, and it is possible to

define intrinsic reactivity for any nucleophile/nucleofuge pair X^-/X^- for any nucleophilic substitution reaction. As for nucleophilic aromatic substitution, S_NAr , vinylic substitution reactions of the $S_NV\pi$ mechanistic variant involve rehybridization from sp^2 in the substrate to sp^3 in the symmetric critical

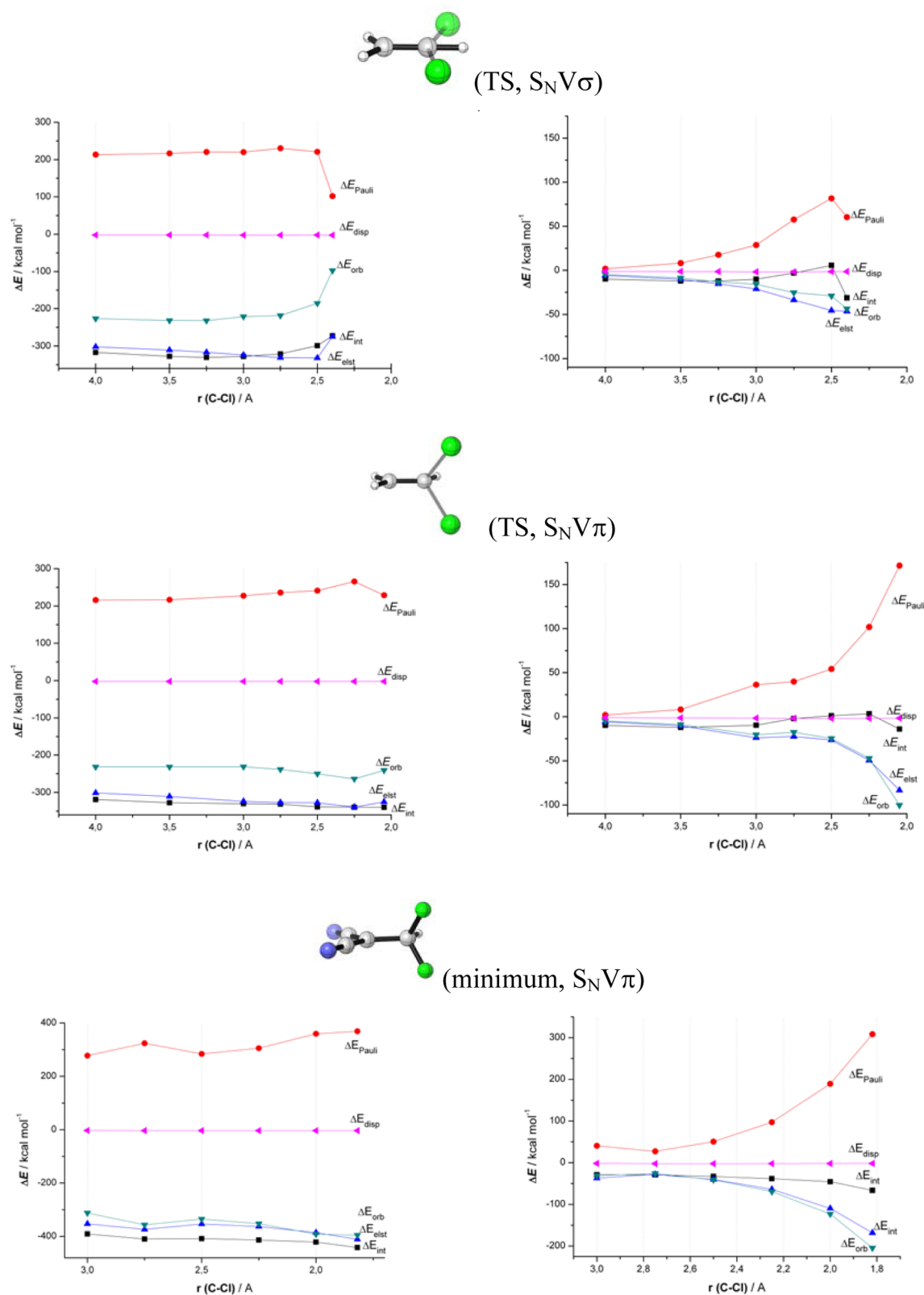


Figure 7. EDA of the interaction energy ΔE_{int} along the reaction coordinate for selected S_NV processes. Left plots: The fragmentation $[\text{R}_2\text{C}=\text{CH}^+] + [\text{Cl}\cdots\text{Cl}]^{2-}$, denoted Reference I in the text. Right plots: the fragmentation $[\text{R}_2\text{C}=\text{CHCl}] + \text{Cl}^-$, denoted Reference II or activation strain model in the text.

configuration in a completely analogous manner. The geometrical arrangement of the critical configuration may correspond to a minimum or a saddle point of the potential energy hypersurface depending on the substrate and the

nucleophile. Intrinsic nucleophilicity in $S_NV\pi$ and S_NAr are therefore essentially equivalent, having very similar electronic requirements, as shown here. Electron withdrawing substituents at the β carbon and/or nucleophile/nucleofuge pairs as found

among the third and fourth row elements facilitate reactivity. A similar result has been found in Alder-ene reactions.⁸⁰ The alternative mechanism, $S_NV\sigma$, is less common for the prototype reactions studied here and is only encountered when the conditions required for $S_NV\pi$ cannot be achieved. However, $S_NV\sigma$ intrinsic reactivity is closely related to aliphatic S_N2 reactivity but is, in general, less responsive since going from sp^2 to sp is more demanding than going from sp^3 to sp^2 . $S_NV\sigma$ barriers decrease if one goes from second- to higher-period nucleophile/nucleofuge pairs. This also agrees well with findings from the ball-in-a-box model that S_N2 barriers go down as the nucleophile/nucleofuge pair has a reduced affinity for the electrophilic carbon atom, which then prefers to reside at a central position in the "box" of the substituents.^{36,37}

All considerations above relate to identity reactions, meaning that any thermodynamic factors have been ignored. Under normal conditions, the nucleophile and the nucleofuge will not be identical, and the thermochemical factor rather than the intrinsic factor becomes more important, the more exothermic the reaction becomes. In the limit of strongly exothermic substitution, it has been noted that the difference in Lewis basicity between the nucleophile and nucleofuge will be the dominating factor.³⁴ In other words, a strong Lewis base is a good nucleophile, and a weak base is a good nucleofuge. This is completely equivalent to the conclusion derived from the activation strain model that a base with a high-energy HOMO is a good nucleophile and a leaving group that binds weakly to carbon in the substrate molecule is a good nucleofuge.^{81,82}

■ ASSOCIATED CONTENT

● Supporting Information

Atom coordinates and absolute energies of calculated structures. This material is available free of charge via the Internet at <http://pubs.acs.org>.

■ AUTHOR INFORMATION

Corresponding Author

*E-mail: einar.uggerud@kjemi.uio.no

Notes

The authors declare no competing financial interest.

■ ACKNOWLEDGMENTS

E.U. is grateful to the Norwegian Research Council for Grant No. 179568/V30 to the Centre of Theoretical and Computational Chemistry through their Centre of Excellence program and the Norwegian Supercomputing Program (NOTUR) through a grant of computer time (Grant No. NN4654K). I.F. acknowledges the Spanish MINECO and CAM (Grants CTQ2010-20714-C02-01, Consolider-Ingenio 2010, CSD2007-00006, and S2009/PPQ-1634). F.M.B. thanks The Netherlands Organization for Scientific Research (NWO-CW) for financial support.

■ REFERENCES

- (1) Smith, M. B.; March, J. *March's Advanced Organic Chemistry: Reactions, Mechanisms, and Structure*, 6 ed.; John Wiley: New York, 2007.
- (2) Loevenich, J.; Losen, J.; Dierichs, A. *Chem. Ber.* **1927**, *60*, 950.
- (3) Hughes, E. D. *J. Chem. Soc., Faraday Trans.* **1941**, *37*, 603.
- (4) Jones, D. E.; Vernon, C. A. *Nature* **1955**, *176*, 791.
- (5) Rappoport, Z. *Adv. Phys. Org. Chem.* **1969**, *7*, 1.
- (6) Modena, G. *Acc. Chem. Res.* **1971**, *4*, 73.

- (7) Testaferri, L.; Tiecco, M.; Tingoli, M.; Chianelli, D. *Tetrahedron* **1985**, *41*, 1401.
- (8) Bernasconi, C. F. *Tetrahedron* **1989**, *45*, 4017.
- (9) Rappoport, Z. *Acc. Chem. Res.* **1992**, *25*, 474.
- (10) Chieffi, A.; Kamikawa, K.; Ahman, J.; Fox, J. M.; Buchwald, S. L. *Org. Lett.* **2001**, *3*, 1897.
- (11) Shiers, J. J.; Shipman, M.; Hayes, J. F.; Slawin, A. M. Z. *J. Am. Chem. Soc.* **2004**, *126*, 6868.
- (12) Poulsen, T. B.; Bernardi, L.; Bell, M.; Jorgensen, K. A. *Angew. Chem., Int. Ed.* **2006**, *45*, 6551.
- (13) Bernasconi, C. F.; Rappoport, Z. *Acc. Chem. Res.* **2009**, *42*, 993.
- (14) Rappoport, Z. *Recl. Trav. Chim. Pays-Bas* **1985**, *104*, 309.
- (15) Stohrer, W. D. *Tetrahedron Lett.* **1975**, *3*, 207.
- (16) Kelsey, D. R.; Bergman, R. G. *J. Am. Chem. Soc.* **1971**, *93*, 1953.
- (17) Strozier, R. W.; Caramella, P.; Houk, K. N. *J. Am. Chem. Soc.* **1979**, *101*.
- (18) Apeloig, Y.; Rappoport, Z. *J. Am. Chem. Soc.* **1979**, *101*, 5095.
- (19) Shainyan, B. A.; Sidorkin, V. F. *Zh. Org. Khim. (USSR)* **1980**, *16*, 3.
- (20) Liotta, C. L.; Burgess, E. M.; Eberhardt, W. H. *J. Am. Chem. Soc.* **1984**, *106*, 4849.
- (21) Bach, R. D.; Wolber, G. J. *J. Am. Chem. Soc.* **1984**, *106*, 1401.
- (22) Cohen, D.; Bar, R.; Shaik, S. S. *J. Am. Chem. Soc.* **1986**, *108*, 231.
- (23) Glukhovtsev, M. N.; Pross, A.; Radom, L. *J. Am. Chem. Soc.* **1994**, *116*, 5961.
- (24) Lucchini, V.; Modena, G.; Pasquato, L. *J. Am. Chem. Soc.* **1995**, *117*, 2297.
- (25) Kim, C. K.; Hyun, K. H.; Kim, C. K.; Lee, I. *J. Am. Chem. Soc.* **2000**, *122*, 2294.
- (26) Bach, R. D.; Baboul, A. G.; Schlegel, H. B. *J. Am. Chem. Soc.* **2001**, *123*, 5787.
- (27) Sączewski, J.; Gdaniec, M. *Eur. J. Org. Chem.* **2010**, *2010*, 2387.
- (28) Miyamoto, K.; Okubo, T.; Hirobe, M.; Kunishima, M.; Ochiai, M. *Tetrahedron* **2010**, *66*, 5819.
- (29) Bogle, X. S.; Singleton, D. A. *Org. Lett.* **2012**, *14*, 2528.
- (30) Laerdahl, J. K.; Civcir, P. U.; Bache-Andreassen, L.; Uggerud, E. *Org. Biomol. Chem.* **2006**, *4*, 135.
- (31) Uggerud, E. *Chem.—Eur. J.* **2006**, *12*, 1127.
- (32) Ochrán, R. A.; Uggerud, E. *Int. J. Mass Spectrom.* **2007**, *265*, 169.
- (33) Fernández, I.; Frenking, G.; Uggerud, E. *Chem.—Eur. J.* **2009**, *15*, 2166.
- (34) Uggerud, E. *Pure Appl. Chem.* **2009**, *81*, 709.
- (35) Pierrefixe, S. C. A. H.; Fonseca Guerra, C.; Bickelhaupt, F. M. *Chem.—Eur. J.* **2008**, *14*, 819.
- (36) Pierrefixe, S. C. A. H.; Poater, J.; Im, C.; Bickelhaupt, F. M. *Chem.—Eur. J.* **2008**, *14*, 6901.
- (37) Pierrefixe, S. C. A. H.; van Stralen, S. J. M.; van Stralen, J. N. P.; Fonseca Guerra, C.; Bickelhaupt, F. M. *Angew. Chem., Int. Ed.* **2009**, *48*, 6469.
- (38) Swart, M.; Sola, M.; Bickelhaupt, F. M. *J. Comput. Chem.* **2007**, *28*, 1551.
- (39) Bento, A. P.; Sola, M.; Bickelhaupt, F. M. *J. Comput. Chem.* **2005**, *26*, 1497.
- (40) Hoz, S.; Basch, H.; Wolk, J. L.; Hoz, T.; Rozental, E. *J. Am. Chem. Soc.* **1999**, *121*, 7724.
- (41) Yi, R.; Basch, H.; Hoz, S. *J. Org. Chem.* **2002**, *67*, 5891.
- (42) Arnaut, L. G.; Formosinho, S. J. *Chem.—Eur. J.* **2008**, *14*, 6578.
- (43) Gonzales, J. M.; Pak, C.; Cox, R. S.; Allen, W. D.; Schaefer, H. F., III; Attila, I. I. I.; Császár, A. G.; Tarczay, G. *Chem.—Eur. J.* **2003**, *9*, 2173.
- (44) Pellerite, M. J.; Brauman, J. I. *J. Am. Chem. Soc.* **1980**, *102*, 5993.
- (45) Wolfe, S.; Mitchell, D. J.; Schlegel, H. B. *J. Am. Chem. Soc.* **1981**, *103*, 7694.
- (46) Dodd, J. A.; Brauman, J. I. *J. Am. Chem. Soc.* **1984**, *106*, 5356.
- (47) Wladkowski, B. D.; Brauman, J. I. *J. Chem. Phys.* **1993**, *97*, 13158.
- (48) Uggerud, E. *J. Chem. Soc., Perkin Trans. 2.* **1999**, 1465–1467.
- (49) Agmon, N. *J. Chem. Soc., Faraday Trans.* **1978**, *74*, 388.

- (50) Mulder, R. J.; Fonseca Guerra, C.; Bickelhaupt, F. M. *J. Phys. Chem. A* **2010**, *114*, 7604.
- (51) Ruiz, J. M.; Mulder, R. J.; Fonseca Guerra, C.; Bickelhaupt, F. M. *J. Comput. Chem.* **2011**, *32*, 681.
- (52) Fernandez, I.; Frenking, G.; Uggerud, E. *J. Org. Chem.* **2010**, *75*, 2971.
- (53) McMahon, T. B.; Heinis, T.; Nicol, G.; Hovey, J. K.; Kebarle, P. *J. Am. Chem. Soc.* **1988**, *110*, 7591.
- (54) McMahon, T. B.; Kebarle, P. *Can. J. Chem.* **1985**, *63*, 3160.
- (55) Uggerud, E. *Eur. Mass Spectrom.* **2000**, *6*, 131.
- (56) Handy, N. C.; Cohen, A. J. *Mol. Phys.* **2001**, *99*, 403.
- (57) Perdew, J. P.; Burke, K.; Ernzerhof, M. *Phys. Rev. Lett.* **1996**, *77*, 3865.
- (58) Swart, M.; Ehlers, A. W.; Lammertsma, K. *Mol. Phys.* **2004**, *102*, 2467.
- (59) Frisch, M. J.; Trucks, G. W.; Schlegel, H. B.; Scuseria, G. E.; Robb, M. A.; Cheeseman, J. R.; Montgomery, J., J. A.; Vreven, T.; Kudin, K. N.; Burant, J. C.; Millam, J. M.; Iyengar, S. S.; Tomasi, J.; Barone, V.; Mennucci, B.; Cossi, M.; Scalmani, G.; Rega, N.; Petersson, G. A.; Nakatsuji, H.; Hada, M.; Ehara, M.; Toyota, K.; Fukuda, R.; Hasegawa, J.; Ishida, M.; Nakajima, T.; Honda, Y.; Kitao, O.; Nakai, H.; Klene, M.; Li, X.; Knox, J. E.; Hratchian, H. P.; Cross, J. B.; Bakken, V.; Adamo, C.; Jaramillo, J.; Gomperts, R.; Stratmann, R. E.; Yazyev, O.; Austin, A. J.; Cammi, R.; Pomelli, C.; Ochterski, J. W.; Ayala, P. Y.; Morokuma, K.; Voth, G. A.; Salvador, P.; Dannenberg, J. J.; Zakrzewski, V. G.; Dapprich, S.; Daniels, A. D.; Strain, M. C.; Farkas, O.; Malick, D. K.; Rabuck, A. D.; Raghavachari, K.; Foresman, J. B.; Ortiz, J. V.; Cui, Q.; Baboul, A. G.; Clifford, S.; Cioslowski, J.; Stefanov, B. B.; Liu, G.; Liashenko, A.; Piskorz, P.; Komaromi, I.; Martin, R. L.; Fox, D. J.; Keith, T.; Al-Laham, M. A.; Peng, C. Y.; Nanayakkara, A.; Challacombe, M.; Gill, P. M. W.; Johnson, B.; Chen, W.; Wong, M. W.; Gonzalez, C.; Pople, J. A.; *Gaussian 04*, revision xx; Gaussian, Inc.: Wallingford CT, 2004.
- (60) Bickelhaupt, F. M. *J. Comput. Chem.* **1999**, *20*, 114.
- (61) van Zeist, W.-J.; Bickelhaupt, F. M. *Org. Biomol. Chem.* **2010**, *8*, 3118.
- (62) Baerends, E. J. et al. *ADF 2007.01*; Scientific Computing & Modelling NV: Amsterdam, The Netherlands, 2007.
- (63) Ziegler, T.; Rauk, A. *Theor. Chim. Acta* **1977**, *46*, 1.
- (64) Morokuma, K. *J. Chem. Phys.* **1971**, *55*, 1236.
- (65) Bickelhaupt, F. M.; Nibbering, N. M. M.; van Wezenbeek, E. M.; Baerends, E. J. *J. Phys. Chem.* **1992**, *96*, 4864.
- (66) Bickelhaupt, F. M.; Diefenbach, A.; de Visser, S. P.; de Koning, L. J.; Nibbering, N. M. M. *J. Phys. Chem. A* **1998**, *102*, 9549.
- (67) Lein, M.; Frenking, G. In *Theory and Applications of Computational Chemistry: The First 40 Years*; Dykstra, C. E., Frenking, G., Kim, K. S., Scuseria, G. E., Eds.; Elsevier: Amsterdam, 2005, p 291.
- (68) Bickelhaupt, F. M.; Baerends, E. J. In *Reviews In Computational Chemistry*; Lipkowitz, K. B., Boyd, D. B., Eds.; Wiley-VCH, Inc: New York, 2000; Vol. 15.
- (69) Velde, G. t.; Bickelhaupt, F. M.; Baerends, E. J.; Guerra, C. F.; Gisbergen, S. J. A. v.; Snijders, J. G.; Ziegler, T. *J. Comput. Chem.* **2001**, *22*, 931.
- (70) Frenking, G.; Wichmann, K.; Fröhlich, N.; Loschen, C.; Lein, M.; Frunzke, J.; Rayón, J. M. *Coord. Chem. Rev.* **2003**, *238–239*, 55.
- (71) Krapp, A.; Bickelhaupt, F. M.; Frenking, G. *Chem.—Eur. J.* **2006**, *12*, 9196.
- (72) Esterhuysen, C.; Frenking, G. *Theor. Chem. Acc.* **2004**, *111*, 381.
- (73) Fernández, I.; Frenking, G. *Chem.—Eur. J.* **2006**, *12*, 3617.
- (74) Hopffgarten, M.; Frenking, G. *WIREs Comp. Mol. Sci.* **2012**, *2*, 43.
- (75) Grimme, S.; Antony, J.; Ehrlich, S.; Krieg, H. *J. Chem. Phys.* **2010**, *132*, 154104.
- (76) Becke, A. D. *Phys. Rev. A* **1988**, *38*, 3098.
- (77) Lee, C.; Yang, W.; Parr, R. G. *Phys. Rev. B* **1988**, *37*, 785.
- (78) van Lenthe, E.; Baerends, E. J.; Snijders, J. G. *J. Chem. Phys.* **1994**, *101*, 9783.
- (79) Schwarz, W. H. E.; Schmidbaur, H. *Chem.—Eur. J.* **2012**, *18*, 4470.
- (80) Fernández, I.; Bickelhaupt, F. M. *J. Comput. Chem.* **2012**, *33*, 509.
- (81) Bento, A. P.; Bickelhaupt, F. M. *J. Org. Chem.* **2008**, *73*, 7290.
- (82) Bento, A. P.; Bickelhaupt, F. M. *Chem. Asian J.* **2008**, *3*, 1783.